Chin. Phys. Lett. **39**, 023301 (2022)

Identification of Above-Threshold Ionization by Imaging Photoelectrons from Ammonia Molecules in an Intense Femtosecond Laser Field

Qin Yang(杨钦)[1,4], Jing Leng(冷静)[1,4], Yan-Hui Wang(王艳辉)[2], Ya-Nan Sun(孙亚楠)[1,3], Hai-Bin Du(杜海滨)[5], Dong-Dong Zhang(张栋栋)[1,4], Le-Le Song(宋乐乐)[1,6], Lan-Hai He(赫兰海)[1,4*], and Fu-Chun Liu(刘福春)[1,4*]

[1]*Institute of Atomic and Molecular Physics, Jilin University, Changchun 130012, China*
[2]*College of Electronic Science and Engineering, State Key Laboratory on Integrated Optoelectronics, Jilin University, Changchun 130012, China*
[3]*Department of Physics, No. 151 Middle School of Changchun, Changchun 130000, China*
[4]*Jilin Provincial Key Laboratory of Applied Atomic and Molecular Spectroscopy, Jilin University, Changchun 130012, China*
[5]*Department of Comprehensive, Harbin City Vocational College, Harbin 150000, China*
[6]*Jilin Institute of Chemical Technology, Jilin 132022, China*

(Received 1 December 2021; accepted 30 December 2021; published online 29 January 2022)

The above-threshold ionization process of ammonia molecules induced by a femtosecond laser field at 800 nm is studied in the intensity range from 1.6×10^{13} to 5.7×10^{13} W/cm^2. Channel switching under different laser intensities is observed and identified in the photoelectron kinetic energy spectra of ammonia. Based on the photoelectron kinetic energy distributions and the photoelectron angular distributions, the characteristic peaks observed are exclusively assigned to the multiphoton resonance through certain intermediate states, followed by multiphoton above-threshold ionization.

DOI: 10.1088/0256-307X/39/2/023301

In the past decades, photoelectron imaging detection technique has gotten better and deeper developments and applications.[1−5] Images of photoelectrons generated in molecular ionization process induced by ultrashort laser pulses is a good way to analyze the ionization mechanisms, involved quantum state, molecular structure and ultra-fast dynamics.[6−10] Ionized photoelectrons carry the information of the involved molecular quantum state and structure. Thus, through studies on the photoelectron kinetic energy distribution (KED) and/or photoelectron angular distribution (PAD), one can access the detailed information on molecular orbitals, structure and dynamics, etc. In addition, ultrashort time scale of femtosecond laser pulses is well suited on investigations of photophysical and photochemical properties for molecular excited states and/or intermediate states within light-matter interaction processes. As early as 1988, Thoman *et al.* proposed the photolysis imaging technique to better study photodissociation and photoionization processes, and extracted structural information of reactant fragments.[11] In 1997, under the efforts of Parker, ion imaging technology was developed into the well-known velocity map imaging (VMI) operation mode, which improved spatial resolution of ion and electron images, by combining ion lens optics and a two-dimensional detector.[12] In 2010, through the femtosecond time-resolved VMI technique, Wang *et al.* studied the multiphoton ionization of nitric oxide and investigated the optical field modulation for Rydberg-state populations.[13] In 2015, Li *et al.* quantitatively analyzed the resonance enhanced multiphoton ionization of Xenon at different laser intensities through VMI technology.[14] Photoelectron velocity imaging is widely applied to research of laser induced atomic and/or molecular ionization, which is the basis for many strong field phenomena, e.g., above-threshold ionization (ATI) processes,[15] high-harmonic generation (HHG),[16−18] laser-induced electron diffraction (LIED),[19,20] holography with photoelectrons,[21,22] tomographic reconstruction of molecular orbital.[23−25] Moreover, combined with control of molecular frame, the corresponding molecular frame PAD would provide additional information of photoionization dynamics.[26−30]

ATI refers to the multiphoton ionization in which the photon-absorption exceeds the minimum number required for ionization. This phenomenon is firstly

*Corresponding authors. Email: lfc@jlu.edu.cn; helanhai@jlu.edu.cn
© 2022 Chinese Physical Society and IOP Publishing Ltd

discovered by Agostini *et al.*[31] The results observed in earlier ATI experiments were explained within perturbation theory. With the successive improvements of the spatial resolution of photoelectron images, it has been found that ATI spectra can present obvious non-perturbation characteristics at relatively high laser intensities.[32,33] Stark shifts of the electronic quantum states will have a significant effect on the ionization threshold and the ionization pathways of the bound electrons. The studies on the multiphoton ATI of atomic samples showed the contribution of resonantly excited states to ionization, which deepened the understanding of the multiphoton ionization behavior of atoms, e.g., Freeman resonance, characteristic angular distributions for the high-order ATI.[34–37] Recently, Li *et al.* systematically studied the ATI of xenon in infrared laser fields.[14,38] These studies indicate that the ATI of atomic samples is consistent with the Freeman resonant picture in a certain extent. However, due to the complex energy level structure, research of the ATI of molecular samples, especially for symmetric top molecules,[39,40] are not yet comprehensively covered either in experiment or in theory, and sufficient experimental data are definitely desired.

As a typical symmetric top molecule, NH_3 is ubiquitous in nature and important in many physical and chemical phenomena.[41–43] Neutral ammonia at its equilibrium configuration has a pyramidal shape, which would undergo a significant geometrical transformation when it is ionized, as the ammonia cation in its ground electronic state has a planar equilibrium geometry.[44] Thus, extensive studies related to the electronic configurations, geometric structures and the corresponding dynamics for ammonia have been conducted. The electronic quantum states, vibrational quantum states, high Rydberg states and rotation quantum states of NH_3 have been extensively investigated in detail using photoelectron spectroscopy and multiphoton ionization spectroscopy.[45–47] In addition, vibrationally mediated photodissociation of NH_3 has been experimentally studied through multiphoton ionization spectroscopies, and the effects of quantum tunneling on the photodissociation dynamics have been observed.[45,48] Furthermore, the geometry-dependent ionization behavior and the ultrafast umbrella motion in ammonia have been visualized with attosecond temporal resolution.[44,49,50] In addition, an ammonia molecule is an essential molecular system in chemistry and atmosphere, and involved in many important reaction processes.[41,51,52] Thus, the detailed studies on the ionization properties for ammonia molecules and the corresponding manipulation would facilitate the ultrafast measurement of related chemical reactions.

In this work, we study ATI processes through VMI technique for the symmetric top molecule NH_3, induced by an 800 nm linear polarized femtosecond laser field. Through the photoelectron spectra of NH_3, the kinetic energy (KE) calibration has been completed. Through the photoelectron KED, we identify several orders of ATI peaks above the kinetic energy of one photon. Moreover, channel switching under different laser intensities is also investigated. The experimental results are consistent with the theoretical analysis. The ATI process of NH_3 and the identification of the involved excited state is further explained and confirmed by the extracted PADs.

The details of the experimental setup have been described in Ref. [47]. Briefly, a Ti:sapphire amplification laser system has been used to generate linearly polarized femtosecond laser pulses (800 nm, 50 fs, 1 kHz and 4 mJ maximum output energy). The polarization direction of the laser is parallel to the detector plane. The laser intensity ranging from 1.6×10^{13} W/cm^2 to 5.7×10^{13} W/cm^2, which was calibrated by measuring the equally spaced ATI peaks of ammonia, has been used during the experiment. The experimental apparatus is divided into two parts: the beam source chamber, and the detection chamber. In the beam source chamber, the molecular beam (1% NH_3 mixed in the neon) is ejected through a pulsed valve (Amsterdam Piezo valve) and then filtered by a skimmer. In the interaction chamber, the laser interacts with the molecular beam in between the repeller and extractor plates of the ion optics, by which the VMI is executed. The generated photoelectrons are collected by a pair of microchannel plates combined with a P47 phosphor screen, from which the signal is captured both by the photomultiplier tube (PMT) to convert into the time-of-flight signal, and a charge-coupled device (CCD) camera to record the 2D distributions. To be noticed, the electrons collected on the detector originate from the single ionization of ammonia under current laser intensity range, which has been checked and monitored with the ion time-of-flight mass spectrum.

The raw photoelectron images of ammonia under three selected laser intensities are shown in Fig. 1, in which the laser field is linearly polarized along the vertical direction. The characteristic channels for these labeled photoelectron peaks are switching under these selected laser intensities, which can be clearly observed. The 3D distribution is extracted through inverse Abel transformation for the raw photoelectron images.[53] Then the KED can be obtained through angular integrations on the transformed photoelectron images, in units of pixels. To obtain a reliable photoelectron KE spectrum, it is necessary to transform the velocity distribution in pixels into KED in eV. The relationship between R and KER (kinetic energy re-

lease) can be written as: $\mathrm{KER}(R) = a_{\mathrm{VMI}}R^2$, in which R is the distance from the imaging center to the observed electron signals (in units of pixels), KER is the KE of the electron at R, a_{VMI} is the converting coefficient. The parameter a_{VMI} depends on the ion optics geometry and the electron time-of-flight t, which is highly sensitive to the voltages on the ion optics and distance between the interaction point to detector. Figure 2 shows the photoelectron KED based on KE calibration of NH_3, compared with the calibration based on the commonly used xenon.[54,55] The difference is small and negligible. Energy calibration with NH_3 can also achieve similar accuracy as xenon.

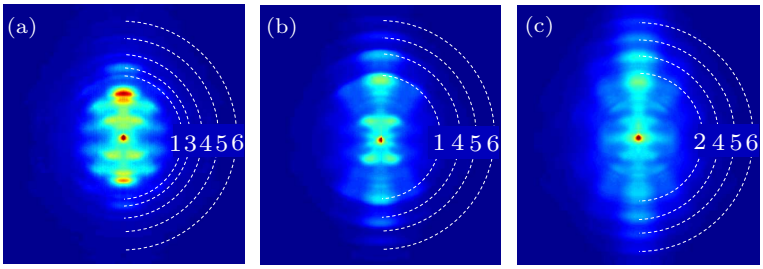

Fig. 1. Raw photoelectron images of NH_3 induced by an 800-nm femtosecond laser. The laser intensities are 1.9, 3.1 and $5.07 \times 10^{13}\,\mathrm{W/cm^2}$ for (a), (b) and (c), respectively. The rings, labeled as 1, 2, 3, 4, 5 and 6, represent the characteristic photoelectron peaks with distinct KEs, observed above one-photon energy.

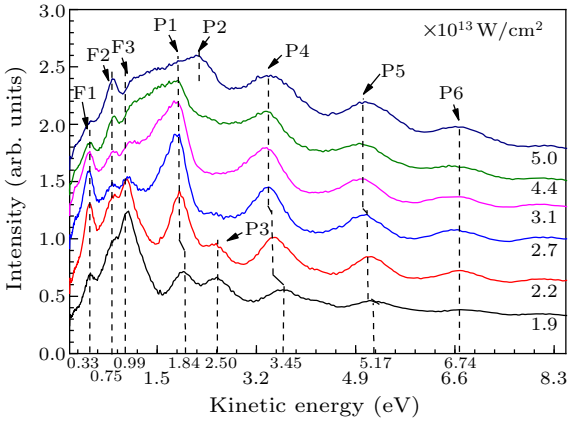

Fig. 2. Calibrated photoelectron KEDs of ammonia under different laser intensities, ranging from 1.9×10^{13} to $5.0 \times 10^{13}\,\mathrm{W/cm^2}$. The characteristic KE peaks are labeled as F1, F2 and F3 in Freeman resonance region, the ATI peaks are labeled as P1, P2, P3, P4, P5 and P6 in the ATI region.

The calibrated KEDs are shown in Fig. 2. In accordance with our previous assignments,[54] there are three characteristic KE peaks (F1, F2 and F3) in Freeman resonance region, which corresponds to the characteristic peaks P1, P2 and P3 in the ATI region. The ATI peaks labeled as P1, P4, P5 and P6 that differ by one-photon energy are energetically equidistant, which indicates these peaks originate from the same resonant excitation pathway and the different orders of ATI process. Furthermore, the peak positions of P1, P4, and P5 slightly shift under different laser intensities. This could be attributed to the non-resonant ionizations contributions besides the resonant excitation/ionization pathways. Within the non-resonance scenario, electrons first absorb certain numbers of photons, and then non-resonantly ionize through the continuum state which would be energetically modified in the order of U_{p} due to Stark effect. Thus, the corresponding kinetic energies of the non-resonant ionized photoelectrons would decrease with the increasing laser intensities. Nevertheless, resonance will greatly enhance the ionization probability of atoms and molecules.[56,57] Thus, we assigned that the observed characteristic peaks mainly originate from resonance excitation/ionization pathways, along with a small fraction of non-resonance ionization resulting in a slight shift of the peak positions. With the variation of laser intensity, the phenomenon of channel switching for the first order of ATI is prominent, similar to that in the Freeman resonance region.[54] The peak P3 dominates the KEDs under relatively low laser intensity, while the peak P1 becomes more pronounced when laser intensity increases from $1.9 \times 10^{13}\,\mathrm{W/cm^2}$ to $2.7 \times 10^{13}\,\mathrm{W/cm^2}$. Peak P2 appears when laser intensity becomes high enough. The channel switching could be interpreted within the concept of Freeman resonance, the specific intermediate states could be populated through resonant excitation under certain laser intensities, and it will be quantitatively analyzed in the following part. Furthermore, the different ratios of populations between characteristic peaks within Freeman resonance region and first-order ATI region have been observed. This may be introduced by the resonance with a certain molecular/ion excited state during the absorption of the last photon above the threshold.

To quantitatively analyze the involved excited states and the corresponding channel switching, we need to calculate the modified vibrational energy levels for different excited states of ammonia molecules introduced by the Stark shifts, which is approximately equal to the ponderomotive potential under different

laser intensities. The $E_A(\nu_2')$, $E_B(\nu_2')$ and $E_C(\nu_2')$ represent the different vibration levels of energy without ponderomotive potentials for A, B and C intermediate states, ν_2' indicated vibration mode in the excited state of NH_3. The vertical ionization energy of ammonia is 10.18 eV, $E_A(0) = 5.73$ eV, $E_B(0) = 7.34$ eV, $E_C(0) = 7.92$ eV for these excited states, respectively.[47] We calculate the modified energies of A, B and C intermediate states ($\nu_2' = 0$) of ammonia molecules by considering the ponderomotive energy U_p (Stark shift) at different laser intensities, as listed in Table 1. In Fig. 3, the upper part shows the modulation of the energy level for the involved excited states of NH_3 in the presence of Stark shift at different laser intensities, and the lower part of Fig. 3 shows the ionization pathways for F1/P1, F2/P2 and F3/P3 peaks with selected laser intensities. Due to the modulation of the energy levels, these excited states would be resonantly populated through multi-photon excitation under certain laser intensities. Combining the upper and lower parts of Fig. 3, the effect of laser field on the channels switching can be clearly visualized. At the laser intensity of 1.9×10^{13} W/cm^2, the B and C excited states are resonantly populated through six-photon excitation, leading to opening of the F1/P1 and F3/P3 channels. The F3/P3 channel is closed at the laser intensity of 3.1×10^{13} W/cm^2. Similarly, at the laser intensity of 5.07×10^{13} W/cm^2, the A excited state is resonantly excited with six photons, and the P2 channel dominants. Moreover, different lifetimes of the involved Rydberg state would affect the channel switching process, depending on if the temporal profile of the laser pulse would cover the lifetime of the involve excited state, from which the electron would be ionized within the same laser pulse. However, the temporal width of the laser pulse in the present experiment is about 50 fs, shorter than the lifetimes of A, B and C excited states which are 100 fs, 8 ps and 10 ps, respectively. Therefore, the A, B and C states could be all resonantly excited and the ionized within one laser pulse.

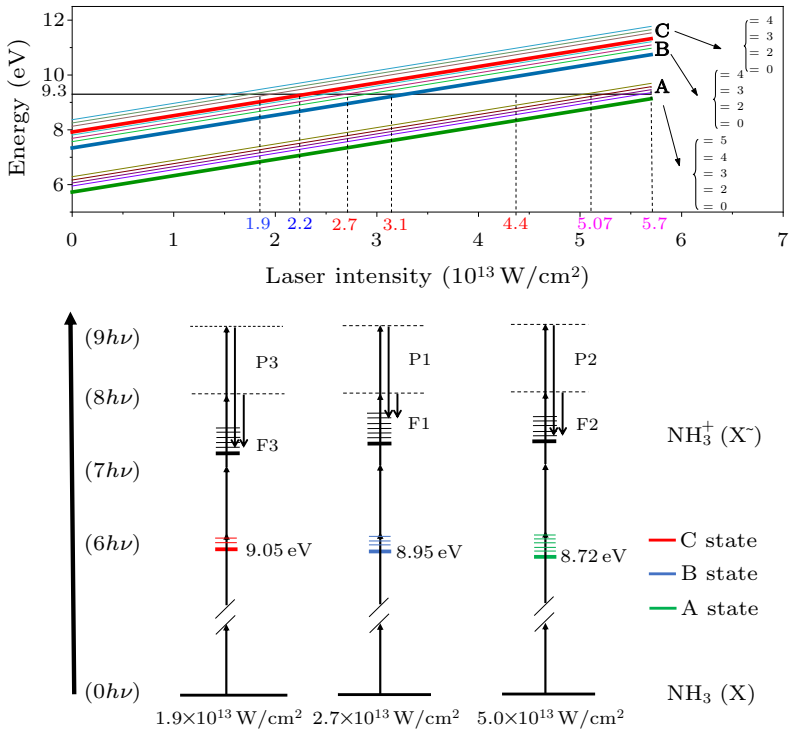

Fig. 3. The upper part shows the modulated energy of the involved intermediate electronic quantum states of NH_3, which are accessible for the absorption of six photons, as a function of laser intensity. The lower part indicates the ionization pathways of F1/P1, F2/P2 and F3/P3 peaks under the laser intensities of 1.9, 2.7 and 5.0×10^{13} W/cm^2, respectively. The thin solid lines above the intermediate states and ionic ground state schematically represent the corresponding vibrational states.

Table 1. Ponderomotive potentials and the modulated energies of A, B and C electronic states ($\nu_2' = 0$) of NH_3, at different laser intensities.

Laser intensity (10^{13} W/cm^2)	1.9	2.2	2.7	3.1	4.4	5.0
U_p (eV)	1.135	1.314	1.612	1.851	2.627	2.986
$E_A = E_A(0) + U_p$	6.865	7.044	7.342	7.581	8.357	8.716
$E_B = E_B(0) + U_p$	8.475	8.654	8.952	9.191	9.967	10.326
$E_C = E_C(0) + U_p$	9.055	9.234	9.712	9.951	10.727	11.086

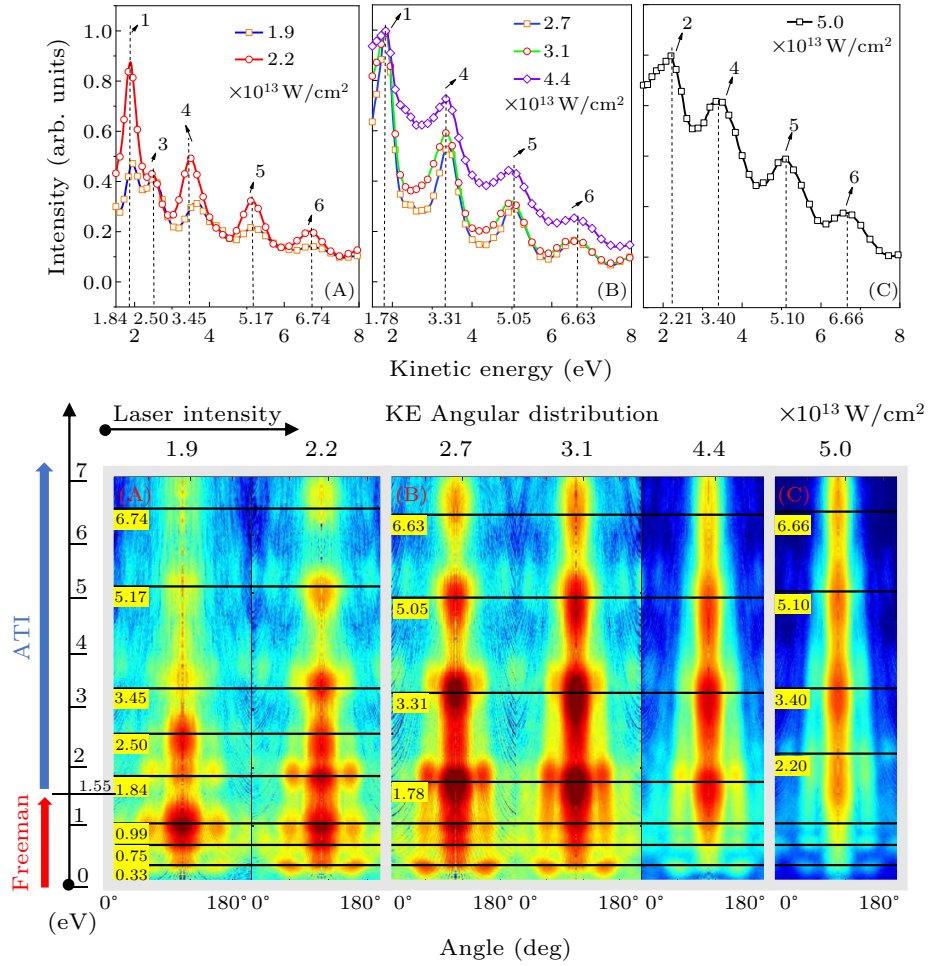

Fig. 4. Upper: the KEDs above the energy of one-photon, in different laser intensity ranges where the channel switching is prominent. Lower: the KE angular-distribution evolving with the increase of laser intensities. (A), (B) and (C) corresponding to the laser intensity ranges from 1.9 to 2.2×10^{13} W/cm^2, 2.7 to 4.4×10^{13} W/cm^2, and at 5.0×10^{13} W/cm^2, respectively.

On the other hand, the KED of photoelectrons is also affected by different involving ion vibrational states in the ionization process. The NH_3 molecules in the laser field will be populated at different vibrational states, resulting in different KEs for the photoelectrons. Based on the vibrational energy level modulation of the ammonia ions, we can extract the main vibrational excitation channels for each peak at different laser intensities. The vibration energy levels listed in Table 2 are calculated via the equation $E_{v_1v_2} = \omega_1(v_1+1/2) - \omega_1\chi_1(v_1+1/2)^2 + \omega_2(v_2+1/2) - \omega_2\chi_2(v_2+1/2)^2$, with $\omega_1 = 3376.6\,\mathrm{cm}^{-1}$, $\omega_1\chi_1 = 23\,\mathrm{cm}^{-1}$, $\omega_2 = 849.3\,\mathrm{cm}^{-1}$, $\omega_2\chi_2 = 16\,\mathrm{cm}^{-1}$.[58] The notation $\nu_1^n\nu_2^m$ represents the given vibrational state, abbreviated as 1^n2^m. Here, n and m denote the corresponding vibrational quantum numbers, ν_1 and ν_2 denote N–H stretching vibration and N–H umbrella vibration in an X state of NH_3^+, respectively.[54,59] To identify the vibrational excitation processes, three characteristic peaks within Freeman resonance regime with the most distinct excitation processes at certain laser intensities are selected in the lower part of Fig. 3, e.g., F1 is the most pronounced signal under the laser intensity of 2.7×10^{13} W/cm^2, which is generated through 6 (photons for resonant excitation) + 2 (photons for ionization) process.[47] In this case, the ammonia molecules are resonantly excited to the intermediate B electronic state inspite of the absorption of six photons (9.3 eV), in accordance with the energy of $\nu_2' = 4$ for B state ($E_B(\nu_2' = 4) = 9.302$ eV) when Stark shift is considered.[60,61] Then, the excited ammonia molecules absorb another two photons during ionization, resulting in a KE of 0.33 eV for the photoelectrons. Thus, a neat energy absorption during excitation/ionization is 12.07 eV, the corresponding ammonia ionic ground states of 1^42^0 (12.05 eV) and/or 1^32^4 (12.04 eV) are most likely populated, when taking the Stark shift into account, as shown in Table 2. Similarly, F2 originates from 6-photon resonant excitation to the vibrational state of $\nu_2' = 5$ for A state ($E_A(\nu_2' = 5) = 9.28$ eV), and 2-photon ionization through the ionic states of 1^32^0 and/or 1^22^4 at the laser intensity of

5.07×10^{13} W/cm^2. F3(P3) originates from 6-photon resonant excitation to the vibrational state of $\nu_2' = 2$ for C state ($E_C(\nu_2' = 2) = 9.27$ eV), and 2-photon ionization through the ionic states of $1^2 2^0$ and/or $1^1 2^4$ at the laser intensity of 1.9×10^{13} W/cm^2. Moreover, the characteristic peaks of P1, P2 and P3, as the first order ATI signals for F1, F2 and F3, originate from the same resonant excitation pathways, followed by an additional photon absorbed during ionization.

Table 2. Ionization energies through different vibrational states between the ground electronic state of neutral ammonia molecule and ammonia cation.

	NH_3^+ (X~)				
Energy (eV)	$v_2 = 0$	$v_2 = 1$	$v_2 = 2$	$v_2 = 3$	$v_2 = 4$
$v_1 = 0$	10.44	10.54	10.64	10.73	10.82
$v_1 = 1$	10.85	10.95	11.04	11.14	11.24
$v_1 = 2$	11.26	11.36	11.46	11.55	11.64
$v_1 = 3$	11.66	11.76	11.86	11.95	12.04
$v_1 = 4$	12.05	12.16	12.26	12.35	12.44

For a better visualization, the above analysis is summarized as the KE angular-distribution plot at different laser intensities, as shown in Fig. 4. The laser intensity ranges for (A), (B), (C) on the two subplots in Fig. 4 are one-to-one correspondence. Channel switching can be directly observed within the KE angular-distribution plot. In the ATI region, P1 and P3 channels are switching to the P2 channel when the laser intensity increases, which is consistent with our previous analysis for F1, F3 and F2 channels in the Freeman region. Thus, the intermediate excited states and channel evolution of ammonia molecules can be observed in a relatively intuitive way through the KE angular-distribution plot. Moreover, the observed main resonant channels through different excited states offer a reference for the quantum state manipulation via modifying the laser intensities.

Combined with the subplots (A), (B), (C) in Fig. 4, and our previous identification of the Freeman resonance peaks,[54] all the ATI peaks P1, P2, P3, P4, P5 and P6 can be identified. In the Freeman resonance region, the peaks F1, F2 and F3 centered at 0.33 eV, 0.75 eV and 0.99 eV are originated by absorbing 6-photon through B, A and C excited states, respectively. Peak P1 centered at 1.84 eV has one-photon energy difference from peak F1, thus it is originated through [6 (number of photons for resonance) + 2 (minimum number for ionization)] + 1 (additional number of photons in the ATI process) multi-photon process mainly passing through the B excited state. Similarly, the peaks P2 and P3 are attributed to (6 + 2) + 1 multi-photon process that mainly through the A and C excited states, respectively. The peaks P4, P5 and P6 are the high order ATIs above peak P1, and can be assigned as (6 + 2) + 2, (6 + 2) + 3 and (6 + 2) + 4 multi-photon process through multiple mixed excited states. For further identification of the multi-photon process through different excited states, we extract the angular distribution for each ATI peak, as shown in Fig. 5. To be noticed, the angular distributions are so strong at 0° and 180°, which show the laser polarization direction. Thus, the signals at 0° and 180° are cut in such a way so as to get a better visualization on the overall PADs structure.

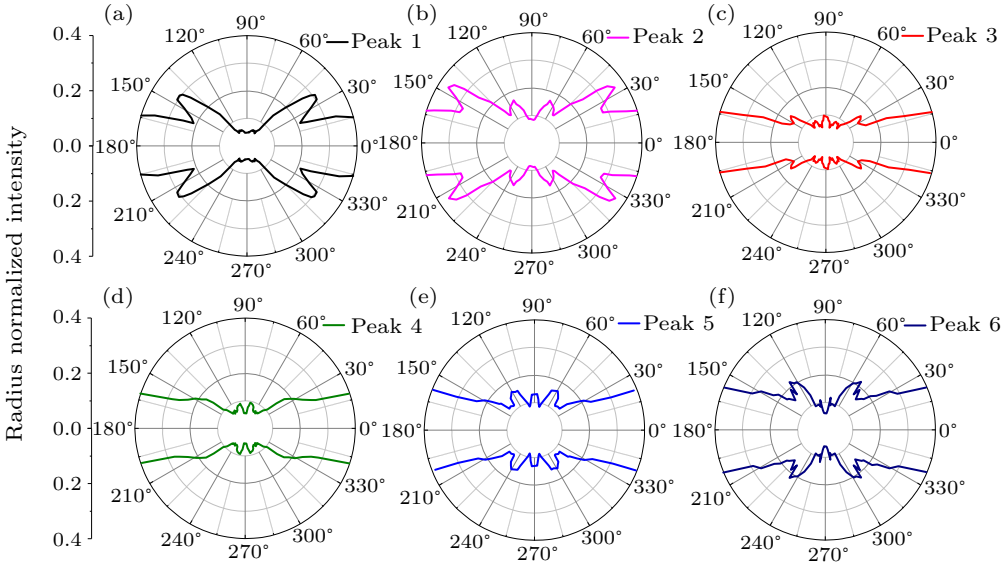

Fig. 5. The PADs of peaks P1(a), P3(c), P4(d), P5(e) and P6(f) extracted from the photoelectron images obtained under the laser intensity of 2.2×10^{13} W/cm^2. The angular distributions of peak P2(b) is extracted from the photoelectron images obtained under the laser intensity of 5.07×10^{13} W/cm^2.

As previously assigned by the KEDs, the peaks P1, P4, P5 and P6 originate from the same intermediate state during resonant excitation process, and just differ by the absorbed photon numbers during ionization. To be noticed, the aim of the PAD analysis is to cross-identify the excitation/ionization pathways during ionization instead of the corresponding cross-sections and dynamics, thus the PADs obtained with isotropically distributed NH_3 samples are sufficient.[62] As is known, the PADs are related to the photoelectron orbital angular momentum.[63,64] With an additional photon absorbed by the sample during ATI process, the orbital angular momentum quantum number will be added by one, which results in a switching of the numbers of the lobes in the PADs. This can be clearly seen from evolution of the lobe structures in the PADs for P4, P5 and P6. However, due to the low signal-to-noise ratio, detailed PAD analysis for peak P1 cannot be performed under current experimental conditions. Furthermore, the observed PADs for P2 and P3 are different. Based on the analysis of the ATI pathways, both of them are generated through two-photon ionization after resonant excitation, which implies that these peaks originate from different intermediate states with distinct orbital angular momentum. This is consistent with the analysis based on the KEDs. The first-order peaks P1, P2 and P3 correspond to the photoelectron KE of three peaks F1, F2 and F3 in the Freeman resonance region, respectively. The ATI peaks P4, P5 and P6 are high-order ATI signals, mainly coming from the resonant excitation via mixed intermediate states.

In summary, the KEDs and PADs of the photoelectrons of NH_3 molecules induced by a femtosecond laser at 800 nm have been experimentally studied and quantitatively analyzed, under the intensity range from 1.6×10^{13} to 5.7×10^{13} W/cm^2. The photoelectron KE spectra of NH_3 have been analyzed in detail under current experimental conditions and four orders of ATI peaks have been observed and assigned. Meanwhile, channel switching phenomena under different laser intensities have been investigated. Combining the analyses for both KEDs and PADs, we can assign the ATI peaks P1, P2 and P3 to a nine-photon process, in which the B, A and C excited states are populated through six-photon resonant excitation, followed by three-photon above-threshold ionization, respectively. Furthermore, the ATI peaks P4, P5 and P6 are high-order ATIs mainly resonant through mixed intermediate states. In this project, the multiphoton ionization processes of ammonia induced by a femtosecond laser are analyzed and identified in detail. The information of KE angular-distributions and channel evolution of NH_3 under different laser intensities related to the intermediate state, ac-Stark effect and multi-orbital effect has been obtained. As a prospect, one can also combine pump-probe technique or two-color field to study the dynamical mechanism of laser induced multiphoton ionization on molecular frame. It can also be used as a reference for molecular selective excitation and quantum control in the molecular reaction dynamics and molecular ionization/dissociation dynamics processes.

Acknowledgements. This work was supported by the National Natural Science Foundation of China (Grant Nos. 11574116, 11534004, 11704147, and 10704028).

References

[1] Aseyev S A, Ni Y, Frasinski L J, Muller H G and Vrakking M J J 2003 *Phys. Rev. Lett.* **91** 223902
[2] Tsubouchi M, Whitaker B J, Wang L, Kohguchi H and Suzuki T 2001 *Phys. Rev. Lett.* **86** 4500
[3] Mauritsson J, Johnsson P, Mansten E, Swoboda M, Ruchon T, L'Huillier A and Schafer K J 2008 *Phys. Rev. Lett.* **100** 073003
[4] Irimia D, Petsalakis I D, Theodorakopoulos G and Janssen M H M 2010 *J. Phys. Chem. A* **114** 3157
[5] Lehmann C S, Ram N B, Powis I and Janssen M H M 2013 *J. Phys. Chem.* **139** 234307
[6] Boll R, Anielski D, Bostedt C, Bozek J D, Christensen L, Coffee R, De S , Decleva P, Epp S W, Erk B, Foucar L, Krasniqi F, Kuepper J, Rouzee A, Rudek B, Rudenko A, Schorb S, Stapelfeldt H, Stener M, Stern S, Techert S, Trippel S, Vrakking M J J, Ullrich J and Rolles D 2013 *Phys. Rev. A* **88** 061402
[7] Ramasesha K, Leone S R and Neumark D M 2016 *Ann. Rev. Phys. Chem.* **67** 41
[8] Ahmed M and Kostko O 2020 *Phys. Chem. Chem. Phys.* **22** 2713
[9] Xiong Y, Wilkin K J and Centurion M 2020 *Phys. Rev. Res.* **2** 043064
[10] Banks H I B, Hadjipittas A and Emmanouilidou A 2020 *J. Phys. B* **53** 225602
[11] Thoman J W, Chandler D W, Parker D H and Janssen M 1988 *Laser Chem.* **9** 27
[12] Eppink A T J B and Parker D H 1998 *Rev. Sci. Instrum.* **68** 3477
[13] Wang B, Liu B, Wang Y and Wang L 2010 *Phys. Rev. A* **81** 043421
[14] Li M, Zhang P, Luo S, Zhou Y, Zhang Q, Lan P and Lu P 2015 *Phys. Rev. A* **92** 063404
[15] Corkum P B 1993 *Phys. Rev. Lett.* **71** 1994
[16] Vampa G, McDonald C R, Orlando G, Klug D D, Corkum P B and Brabec T 2014 *Phys. Rev. Lett.* **113** 073901
[17] Shao J, Zhang C P, Jia J C, Ma J L and Miao X Y 2019 *Chin. Phys. Lett.* **36** 054203
[18] Zhang H, Liu X, Jin F, Zhu M, Yang S, Dong W, Song X and Yang W 2021 *Chin. Phys. Lett.* **38** 063201
[19] Meckel M, Comtois D, Zeidler D, Staudte A, Pavicic D, Bandulet H C, Pepin H, Kieffer J C, Doerner R, Villeneuve D M and Corkum P B 2008 *Science* **320** 1478
[20] Blaga C I, Xu J, DiChiara A D, Sistrunk E, Zhang K, Agostini P, Miller T A, DiMauro L F and Lin C D 2012 *Nature* **483** 194
[21] Bian X B, Huismans Y, Smirnova O, Yuan K J, Vrakking M J J and Bandrauk A D 2011 *Phys. Rev. A* **84** 043420
[22] Wang S, Zhu Z, Zhang Y, Yan T M and Jiang Y 2021 *Chin. Phys. Lett.* **38** 013401

[23] van der Zwan E V, Chirila C C and Lein M 2008 *Phys. Rev. A* **78** 033410
[24] Smeenk C, Arissian L, Staudte A, Villeneuve D M and Corkum P B 2009 *J. Phys. B* **42** 185402
[25] Holmegaard L, Hansen J L, Kalhoj L, Kragh S L, Stapelfeldt H, Filsinger F, Kuepper J, Meijer G, Dimitrovski D, Abu-samha M, Martiny C P J and Madsen L B 2010 *Nat. Phys.* **6** 428
[26] Allendorf S W, Leahy D J, Jacobs D C and Zare R N 1989 *J. Chem. Phys.* **91** 2216
[27] Townsend D and Reid K L 2000 *J. Chem. Phys.* **112** 9783
[28] Stapelfeldt H and Seideman T 2003 *Rev. Mod. Phys.* **75** 543
[29] Yin Y Y, Chen C, Elliott D S *et al.* 1992 *Phys. Rev. Lett.* **69** 2353
[30] Dong D P, Yang B H, Qian D B, Zhou W C, Zhang S F and Ma X 2021 *Chin. Phys. Lett.* **38** 083301
[31] Agostini P, Fabre F, Mainfray G, Petite G and Rahman N K 1979 *Phys. Rev. Lett.* **42** 1127
[32] Agostini P, Kupersztych J, Lompré L, Petite G and Yergeau A 1987 *Phys. Rev. A* **36** 4111
[33] Bashkansky M, Bucksbaum P H and Schumacher D W 1988 *Phys. Rev. Lett.* **60** 2458
[34] Kruit P, Kimman J, Muller H G and van der Wiel M J 1983 *Phys. Rev. A* **28** 248
[35] Freeman R R, Bucks B U P H, Milchberg H, Darack S, Schumacher D and Geusic M E 1987 *Phys. Rev. Lett.* **59** 1092
[36] Guo D S and Drake G 1992 *Phys. Rev. A* **45** 6622
[37] Nandor M J, Walker M A and Van Woerkom L D 1998 *American Physical Society, DAMOP Meeting*, 27–30 May 1998, Santa Fe, New Mexico, p C1.02
[38] Min L, Geng J W, Hong L, Deng Y, Wu C, Peng L Y, Gong Q and Liu Y 2014 *Phys. Rev. Lett.* **112** 113002
[39] Stephens S L, Walker N R and Legon A C 2011 *Phys. Chem. Chem. Phys.* **13** 20736
[40] Luo S, Hu W, Yu J, Li X, He L, Wang C, Liu F and Ding D 2017 *J. Phys. Chem. A* **121** 6547
[41] Suzuki H, Yamamoto S, Ohishi M, Kaifu N and Takano S 1992 *Astrophys. J.* **392** 551
[42] Cavaliere S, Hannauer J, Demirci U B, Akdim O and Miele P 2011 *Catal. Today* **170** 3
[43] Queyroux J A, Ninet S, Weck G, Garbarino G, Plisson T, Mezouar M and Datchi F 2019 *Phys. Rev. B* **99** 134107
[44] Kraus P M and Woerner H J 2013 *ChemPhysChem* **14** 1445
[45] Ashfold M, Dixon R N and Stickland R J 1984 *Chem. Phys.* **88** 463
[46] Sarka K and Schrötter H W 1996 *J. Mol. Spectrosc.* **179** 195
[47] Song L L, Sun Y N, Wang Y H, Wang X C, He L H, Luo S Z, Hu W H, Tong Q N, Ding D J and Liu F C 2019 *Chin. Phys. B* **28** 063201
[48] Hui Y, Evans N L, Chatterley A S, Roberts G M and Ullrich S 2014 *J. Phys. Chem. A* **118** 9438
[49] Foerster J, Plesiat E, Magana A and Saenz A 2016 *Phys. Rev. A* **94** 043405
[50] Belsa B, Amini K, Liu X, Sanchez A and Biegert J 2021 *Struct. Dyn.* **8** 014301
[51] Corchado J C, Espinosa-Garcia J and Yang M 2011 *J. Chem. Phys.* **135** 014303
[52] Sun Y, Wang H, He Z, Qiao B and Chen X 2021 *Phys. Chem. Chem. Phys.* **23** 4856
[53] Apostolopoulos M I, Taroudakis M I and Papazoglou D G 2013 *Opt. Commun.* **296** 25
[54] Sun Y N, Wang Y H, Song L L, Du H B and Liu F C 2020 *Chin. Phys. B* **29** 093201
[55] Tolliver J, Zahedpour S, Wahlstrand J K, Milchberg H M and Kolesik M 2020 *Opt. Lett.* **45** 5780
[56] Charron E, Sukharev M and Suzor-Weiner A 2004 *Laser Phys. Lett.* **1** 18
[57] Nolde M, Weitzel K M and Western C M 2005 *Phys. Chem. Chem. Phys.* **7** 1527
[58] Xie J, Jiang B, Li G, Yang S, Xu J, Sha G, Xu D, Lou N and Zhang C 2000 *Faraday Discuss.* **115** 127
[59] Vaida V, Mccarthy M I, Engelking P C, Rosmus P, Werner H J and Botschwina P 1987 *J. Chem. Phys.* **86** 6669
[60] Nieman G C and Colson S D 1979 *J. Chem. Phys.* **71** 571
[61] Glownia J H, Riley S J, Colson S D and Nieman G C 1980 *J. Chem. Phys.* **73** 4296
[62] Reid K L 2003 *Ann. Rev. Phys. Chem.* **54** 397
[63] Deng Y, Liu Y, Liu X, Liu H, Yang Y, Wu C and Gong Q 2011 *Phys. Rev. A* **84** 65405
[64] Liu Y, Gerber T, Radi P, Sych Y and Knopp G 2014 *Chem. Phys. Lett.* **610** 153